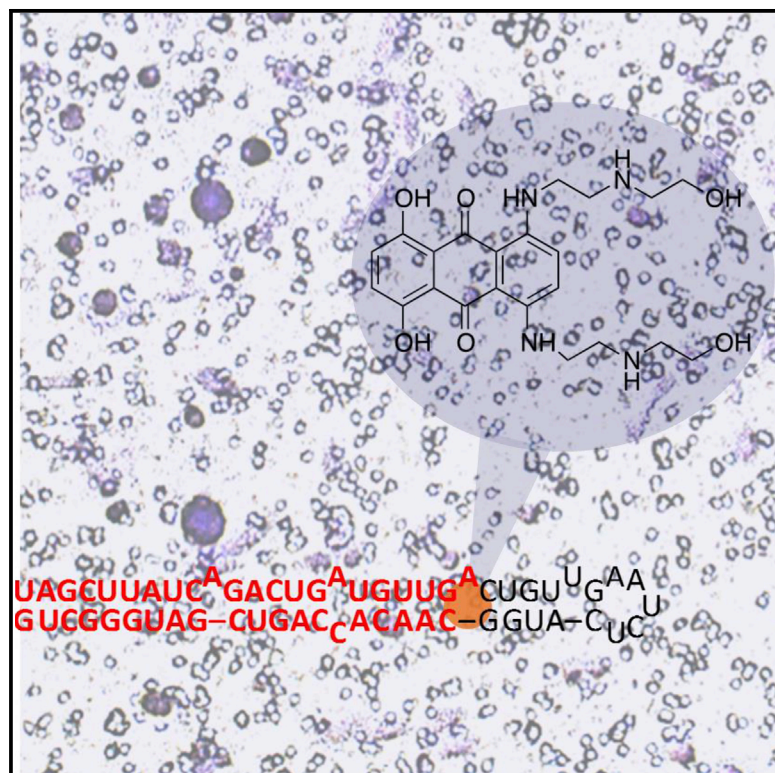


Cell Chemical Biology

Approved Anti-cancer Drugs Target Oncogenic Non-coding RNAs

Graphical Abstract



Authors

Sai Pradeep Velagapudi,
Matthew G. Costales,
Balayeshwanth R. Vummidi, ...,
Arnab K. Chatterjee,
Jessica L. Childs-Disney,
Matthew D. Disney

Correspondence

disney@scripps.edu

In Brief

RNA is an emerging target for small molecules, but has it been an established one all along? Velagapudi et al. profiled the binding of medicines to thousands of RNA motifs, showing that broad drug classes bind RNA. Indeed, approved anti-cancer drugs target an oncogenic non-coding RNA, affecting its phenotype.

Highlights

- Broad classes of small molecule medicines bind RNA
- Sequence-based design shows that approved medicines target oncogenic microRNA-21
- The medicines target microRNA-21 in cells, reversing phenotype in cancer cells
- Oncogenic non-coding RNAs could be an established drug target all along

Approved Anti-cancer Drugs Target Oncogenic Non-coding RNAs

Sai Pradeep Velagapudi,¹ Matthew G. Costales,¹ Balayeshwanth R. Vummidi,¹ Yoshio Nakai,¹ Alicia J. Angelbello,¹ Tuan Tran,¹ Hafeez S. Haniff,¹ Yasumasa Matsumoto,¹ Zi Fu Wang,¹ Arnab K. Chatterjee,² Jessica L. Childs-Disney,¹ and Matthew D. Disney^{1,3,*}

¹Department of Chemistry, The Scripps Research Institute, 130 Scripps Way, Jupiter, FL 33458, USA

²California Institute for Biomedical Research (CALIBR), 11119 North Torrey Pines Road, Suite 100, La Jolla, CA 92037, USA

³Lead Contact

*Correspondence: disney@scripps.edu

<https://doi.org/10.1016/j.chembiol.2018.05.015>

SUMMARY

Potential RNA drug targets for small molecules are found throughout the human transcriptome, yet small molecules known to elicit a pharmacological response by directly targeting RNA are limited to antibacterials. Herein, we describe AbsorbArray, a small molecule microarray-based approach that allows for unmodified compounds, including FDA-approved drugs, to be probed for binding to RNA motif libraries in a massively parallel format. Several drug classes bind RNA including kinase and topoisomerase inhibitors. The latter avidly bound the motif found in the Dicer site of oncogenic microRNA (miR)-21 and inhibited its processing both *in vitro* and in cells. The most potent compound de-repressed a downstream protein target and inhibited a miR-21-mediated invasive phenotype. The compound's activity was ablated upon overexpression of pre-miR-21. Target validation via chemical crosslinking and isolation by pull-down showed direct engagement of pre-miR-21 by the small molecule in cells, demonstrating that RNAs should indeed be considered druggable.

INTRODUCTION

RNA plays important roles in nearly every cellular process and its dysregulation can contribute to disease (Calin and Croce, 2006; Cooper et al., 2009). The Encyclopedia of DNA Elements (ENCODE) project and subsequent analyses showed that only 1%–2% of our genome encodes for protein, yet ca. 80% of it is transcribed into RNA (ENCODE Project Consortium, 2012). Although the amount of functional non-coding RNAs is controversial, it is clear that they carry out essential cellular functions.

The development of therapeutics that target RNA has mostly centered on using oligonucleotides. They are invaluable tools that have been advanced to multiple clinical trials. For example, in late 2016 an antisense agent was approved to treat spinal muscular atrophy, a devastating and heretofore incurable disease (Morrow, 2017). When antisense oligonucleotides are not

directly delivered to the CNS, however, side effects have been observed, ranging from stimulating an immune response to thrombocytopenia (Frazier, 2015).

Small molecules could be a preferred modality for targeting RNA; however, these compounds have been generally limited to antibiotics that target the three-dimensional structure of the ribosome (Blount and Breaker, 2006; Poehlsgaard and Douthwaite, 2005; Tenson and Mankin, 2006) or riboswitches (Blount and Breaker, 2006). Indeed, compounds targeting nucleic acids, including antisense, are known to bind to proteins as well (Ivanov et al., 1998; Liang et al., 2015). Compounds have been identified to target RNA by using various methods including screening, structure-based design, and sequence-based design, cementing RNA as a potentially broad small molecule drug target. One class of non-coding RNAs that has been extensively targeted by small molecules are viral RNAs. The first viral RNA regulatory elements shown to be bound and interfered with by small molecules were the HIV transactivation response (Mei et al., 1995) and Rev response element (Zapp et al., 1993). Other viral RNAs, such as the hepatitis C virus internal ribosomal entry site and influenza A, have been focus of several targeting studies (Dibrov et al., 2014; Lee et al., 2014). Recently, several small molecules have been designed to target nucleotide repeat expansions including fragile X-associated tremor ataxia syndrome (CGG) (Yang et al., 2016), myotonic dystrophy type 1 (CUG) (Gareiss et al., 2008; Jahromi et al., 2013; Pushechnikov et al., 2009), myotonic dystrophy type 2 (CCUG) (Childs-Disney et al., 2014), Huntington's disease (CAG) (Kumar et al., 2012), and frontotemporal dementia and amyotrophic lateral sclerosis (G₄C₂) (Su et al., 2014). A salient question is if small molecules that target non-coding RNAs can be identified and developed into medicines or chemical probes.

A way to evaluate the druggability of RNA is to study if known drugs bind it and affect physiologically important pathways. Perhaps non-coding human RNAs are targeted with approved drugs in their clinical settings, but these interactions have gone unidentified. The focus of this work is to study the potential of RNA as a small molecule drug target using known drug classes. Unmodified drugs were probed for binding RNA motifs using a non-covalent small-molecule microarray (AbsorbArray) in a massively parallel library-versus-library screening approach dubbed two-dimensional combinatorial screening (2DCS) (Childs-Disney et al., 2007; Disney et al., 2008). Indeed, various drug classes including kinase inhibitors, pre-mRNA splicing

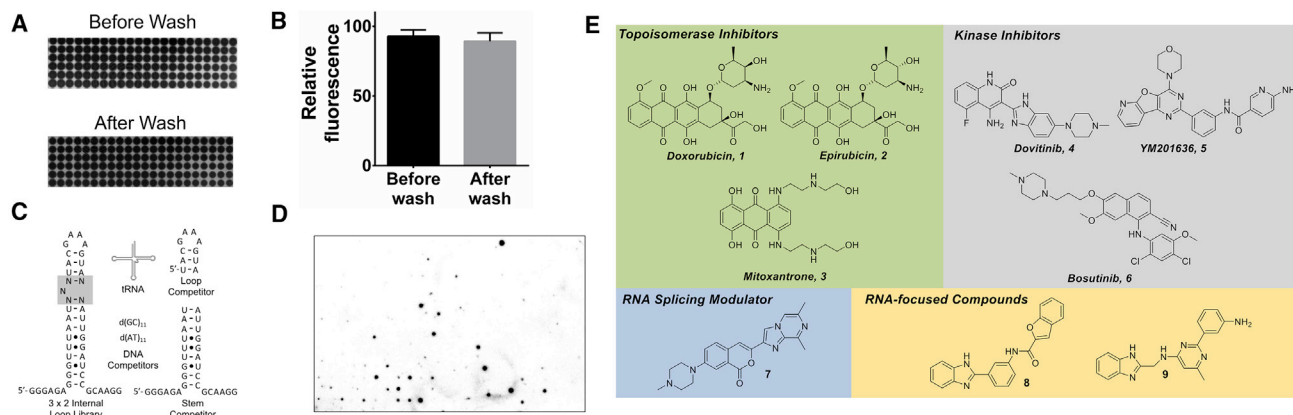


Figure 1. The Development of AbsorbArray and the RNA Motif Libraries Used to Study Small Molecule Binding

(A) Representative image of an AbsorbArray chip after spotting mitoxantrone before and after washing. (B) Plot of the signal from mitoxantrone before and after washing. (C) Secondary structures of the nucleic acids used in this study. (D) Representative image of an AbsorbArray-enabled 2DCS screen (85.5 × 127.8 × 1.1 mm; width × height × thickness). (E) Structures of various small molecules that are found to bind RNA in this AbsorbArray-enabled 2DCS experiment. See also Figure S1 and Table S1.

modulators, and topoisomerase inhibitors bound RNA avidly. By mining Inforna, a sequence-based lead identification strategy for RNA (Velagapudi et al., 2014), it was found that topoisomerase inhibitors bound the Dicer site of the microRNA (miR)-21 precursor (pre-miR-21). In cells, these compounds reduced mature miR-21 levels and modulated a miR-21-mediated invasive phenotype, as miR-21 is oncogenic. Importantly, chemical crosslinking and isolation by pull-down (Chem-CLIP) (Guan and Disney, 2013; Rzuczek et al., 2017; Yang et al., 2015) studies revealed physical interactions between pre-miR-21 and the small molecule.

RESULTS

Development of AbsorbArray

To develop an approach that allowed for unmodified compound libraries to be probed for binding to a library of RNA motifs, we looked to advances in small molecule microarrays. Small molecule microarrays have been invaluable tools to identify compounds that bind biomolecules; however, compounds are immobilized by adding functional groups that allow for covalent attachment (Hergenrother et al., 2000; MacBeath et al., 1999; MacBeath and Schreiber, 2000). Such modifications could affect molecular recognition of the parent compound's natural targets. Herein, we describe an approach named AbsorbArray (Figure 1) that allows small molecules to be non-covalently adhered onto a surface and probed for binding to a library of RNA motifs found in non-coding RNAs. By testing various conditions, we found that small molecules can be absorbed onto hydrated agarose-coated microarray surfaces that are subsequently dried (Figure S1).

Identification of Small Molecules that Bind RNA Motifs via AbsorbArray and 2DCS

AbsorbArray allows for unmodified small molecules to be retained on a surface after washing (Figures 1A and 1B) and then

probed for binding to radiolabeled RNA motif libraries (Figures 1C and 1D). To validate the platform, we probed the binding of the following compounds to RNA motifs via AbsorbArray and 2DCS (Disney et al., 2008): the NIH Clinical Collection (NIH-CC), a library of 727 pharmacologically active compounds used in human clinical trials; kinase inhibitors known to modulate RNA biology but not known to directly engage RNA (SYNlibrary95, Synkinase; n = 95); an RNA-focused library (n = 201) (Rzuczek et al., 2015); and three compounds that modulate the alternative splicing of survival motor neuron 2 (Naryshkin et al., 2014; Palacino et al., 2015). As many of the compounds in these studies have been used in clinical trials, they provide a potentially rich source of drugs that can be re-purposed to target RNA.

In brief, the array was hybridized with a ³²P-labeled RNA library displaying randomized nucleotides in the pattern of a 3 × 2 nucleotide internal loop (3 × 2 ILL; Figure 1C). The 1,024 member 3 × 2 ILL was chosen as it contains asymmetric ILLs and bulges present in various cellular RNAs that are of high importance, as described previously via a transcriptome-wide RNA structural analysis (Liu et al., 2016). Incubation was completed in the presence of excess oligonucleotides that include tRNA, DNA, and mimics of the regions common to all library members (Figure 1C), ensuring interaction of the small molecules with the randomized region (Figure 1D). These studies defined a series of compounds and compound classes as RNA binders (Figure 1D), including topoisomerase inhibitors, kinase inhibitors, and splicing modulators (Figure 1E). Importantly, several unique small molecules (hits derived from the RNA-focused library) were discovered using this platform (Figure 1E).

The RNA motifs from 3 × 2 ILL that bound each compound were harvested from the array surface and sequenced. To score the relative affinities of the selected RNA motifs, an approach called high-throughput structure-activity relationships through sequencing (HiT-StARTS) was applied (Velagapudi et al., 2017). In HiT-StARTS, the frequency of each RNA bound to a small molecule is compared with its frequency in the starting

Table 1. Global Analysis of Selected RNA Motif-Small Molecule Interactions and Binding Affinities of Topoisomerase Inhibitors to the A Bulge in the Dicer Site of pre-miR-21 and the Corresponding Fully Paired RNA

Compound	Range of Z_{obs} for Binders	No. of Binders	Range of K_d Values for Binders (nM)	A Bulge	Base Paired Control
1	28–8	371	20–550	58 ± 7.6	>1000
2	37–8	281	6–35	24 ± 8.1	1080 ± 231
3	39–8	213	10–26	33 ± 3.3	>1000

K_d values are reported in nM. See also Figure S2 and Table S1.

library, as determined by RNA-seq analysis. This pooled population comparison quantifies the statistical significance of enrichment, or the parameter Z_{obs} . HiT-STARTS quickly identifies binding and non-binding RNA motifs for a specific small molecule and minimizes false negatives and positives. Binding assays were completed between selected RNA motif-small molecule pairs, revealing high affinity and selective binding when $Z_{obs} > 8$ (Table 1), as observed previously (Velagapudi et al., 2017) and highlighting the predictive value of HiT-STARTS. Fitness scores are assigned for RNA binders by normalizing Z_{obs} values to the highest Z_{obs} for a given selection, with the best score assigned a value of 100 (Velagapudi et al., 2014).

Inforna Identifies Oncogenic miRNA Targets from AbsorbArray

The RNA motifs identified by 2DCS of the NIH-CC were mined against the RNA motifs in all human miRNA precursors (Velagapudi et al., 2014) to identify potential oncogenic miRNA targets. Several compounds were predicted to bind Drosha or Dicer processing sites (Table S1). To further refine the RNA targets, we compared the relative expression profiles of the potential miRNA hits (Table S1) from publicly available databases using miRmine (Panwar et al., 2017). miR-21 was found to be expressed at 30- to 4,000-fold higher expression compared with other potential miRNA targets. As the oncomiR is upregulated in most cancers (Volinia et al., 2006), contributes to various cancer phenotypes (Chan et al., 2005; du Rieu et al., 2010; Meng et al., 2007; Seike

et al., 2009; Yan et al., 2008), and has been a focus of various small molecule targeting efforts, miR-21 was further studied.

Inforna identified that topoisomerase inhibitors **1**, **2**, and **3** bind the A bulge in the Dicer site of the miR-21 hairpin precursor (Figure 2A). Compounds **1** and **3** were previously observed to stabilize single-stranded regions of RNA by nuclear magnetic resonance (NMR) spectroscopy (Marcheschi et al., 2009; Zheng et al., 2009), supporting the hypothesis that these compounds can bind to the A bulge. We therefore measured the affinity of each compound to the A bulge of miR-21 (Figure S2), affording K_d values of 58 ± 7.6 , 24 ± 8.1 , and 33 ± 3.3 nM for **1**, **2**, and **3**, respectively (Table 1; Figure S2B). Notably, binding was not saturable for compounds **1** and **3** to a fully base paired RNA up to 5,000 nM; binding of **2** to the fully paired RNA was 28-fold weaker than to the A bulge, with a K_d of $1,080 \pm 231$ nM (Table 1; Figure S2C). Interestingly, **3** also binds the U bulge adjacent to the Dicer site with high affinity, as predicted by Inforna, with a dissociation constant of 46 ± 7.1 nM. Increased avidity of **3** is observed to an RNA that contains both the A and U bulges ($K_d = 22 \pm 8.3$ nM) (Figure S2). Despite the dynamics of RNA structure, both the A and U bulge regions in the miR-21 hairpin precursor have been observed by NMR spectroscopy (Chirayil et al., 2014). Additional binding analyses, using microscale thermophoresis (Moon et al., 2018; Seidel et al., 2013), indicated the binding affinity of **3** to a miR-21 hairpin containing both the A and U bulge (miR-21 Hairpin, Figure S2D) and a miR-21 hairpin containing only the A bulge (miR-21 A Bulge, Figure S2E) as 500 and

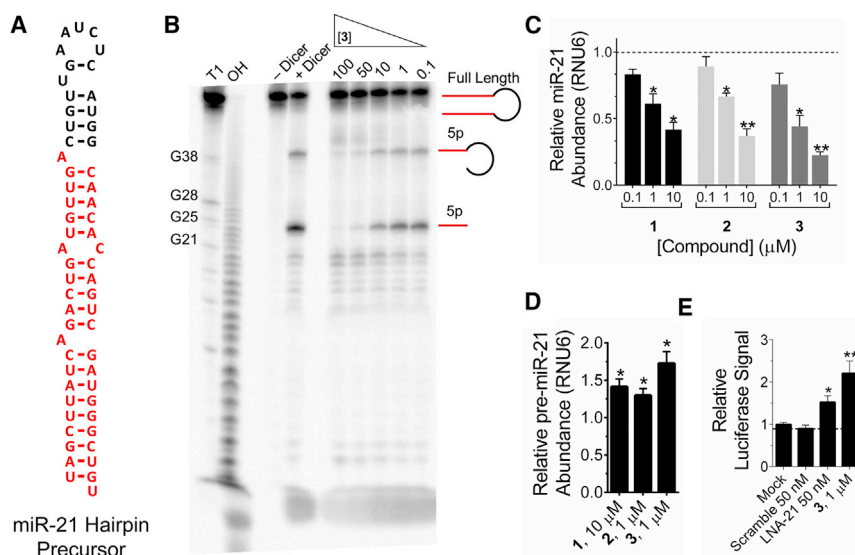


Figure 2. Inhibition of Dicer Processing of pre-miR-21 In Vitro and in Cells

(A) Secondary structure of the miR-21 hairpin precursor.

(B) Representative gel image of the inhibition of Dicer processing of pre-miR-21 by **3**.

(C) Effect of **1**, **2**, and **3** on mature levels in triple negative breast cancer cell line MDA-MB-231.

(D) Effect of **1**, **2**, and **3** on pre-miR-21 levels in triple negative breast cancer cell line MDA-MB-231.

(E) Effect of **3**, an LNA oligonucleotide targeting miR-21 (LNA-21; Exiqon, 4100689-101), and a control LNA (Scramble; Exiqon, 199006-102) on PTEN using a luciferase reporter assay.

* $p < 0.05$, ** $p < 0.01$, as determined by a two-tailed Student t test. Data represent means \pm SEM of biological triplicates. See also Figures S2 and S3.

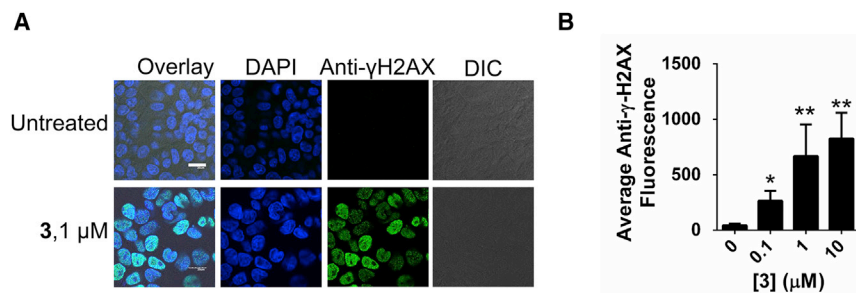


Figure 3. Effect of 3 on DNA Damage

(A) Representative confocal microscopy images of the effect of 3 on DNA damage in MDA-MB-231 cells by staining for γ-H2AX foci. Scale bar, 20 μm.

(B) Quantification of DNA damage upon treatment of MDA-MB-231 cells with 3. *p < 0.05, **p < 0.01, as determined by a two-tailed Student t test.

Data represent mean ± SD of fluorescence intensity across eight images. See also Figure S4.

300 nM, respectively. Notably, no binding was observed to a miR-21 base pair control without the A and U bulges (miR-21 Base Pair, Figure S2F). As 3 showed high affinity for both the A and U bulges found in miR-21, compound 3 was tested for inhibition of pre-miR-21 Dicer processing *in vitro*. A dose response was observed with a half maximal inhibitory concentration (IC₅₀) of ~3 μM (Figure 2B). We next completed a mutational analysis to study the effect of small molecule binding to both bulges. Removing the A bulge at the Dicer site (pre-miR-21 A22 mutant) significantly ablates compound activity while removing the U bulge (pre-miR-21 U27 mutant) does not (Figure S3). These studies also show that 3 does not globally (non-selectively) inhibit Dicer enzyme activity (Figure S3). Thus, this class of compounds, known to affect cellular processes by targeting DNA (Binaschi et al., 1995), might also elicit anti-cancer effects by affecting the biogenesis of miR-21.

Activity of Lead Compounds

Compounds 1, 2, and 3 are readily taken up into cells and localize in both the cytoplasm and nucleus (Feofanov et al., 1997; Shaull et al., 2013). Therefore, the efficacy of the topoisomerase inhibitors for inhibiting biogenesis of miR-21 was tested in the triple-negative breast cancer cell line MDA-MB-231 by measuring mature and pre-miR-21 levels by qRT-PCR. Indeed, all three compounds reduced levels of the mature miR-21 (Figure 2C) and increased levels of pre-miR-21 (Figure 2D). The IC₅₀ values for 1, 2, and 3 for reducing mature miR-21 levels are approximately 5, 10, and 1 μM, respectively. As 3 most significantly increased pre-miR-21 levels (Figure 2D), it was further characterized for de-repressing a downstream protein target. Indeed, 3 de-repressed the downstream effect of miR-21 on the tumor

suppressor phosphatase and tensin homolog deleted on chromosome 10 (PTEN) (Li et al., 1997), using a previously validated luciferase reporter (O'Donnell et al., 2005) (Figure 2E).

The most widely accepted mode of action for 3 is DNA intercalation, leading to crosslinks and strand breaks (Lown et al., 1984). We therefore studied if the concentration required to reduce mature miR-21 levels also causes DNA damage. DNA damage was assessed by imaging γ-H2AX foci that form in response to DNA double-strand breaks (Pilch et al., 2003; Rogakou et al., 1999). These studies showed that both DNA damage and a reduction of miR-21 levels were observed at the active concentration of 1 μM (Figures 3 and S4A). We also tested the effect of 3 on topoisomerase II activity *in vitro* and found an inhibitory effect of 3 at 1 μM (Figures S4B–S4D).

Compound 3 Inhibits an miR-21-Mediated Invasive Phenotype

As previous studies have shown that miR-21 contributes to a migratory and invasive phenotype (Huang et al., 2009; Zhu et al., 2008), we next studied if inhibition of miR-21 by 3 was sufficient to induce a reversal of phenotype in MDA-MB-231 cells by using a Boyden chamber assay. Dose-dependent inhibition of invasive phenotype was observed (Figures 4A and 4B). Importantly, the activity of 3 against an invasive phenotype is ablated by overexpression of pre-miR-21 (Figure 4C), indicating that the effect is via a miR-21-mediated circuit.

Compound 3 Binds pre-miR-21 in Cells as Determined by Chem-CLIP

To further evaluate whether 3 directly engages pre-miR-21 in cells, we used Chem-CLIP, a small molecule-RNA profiling

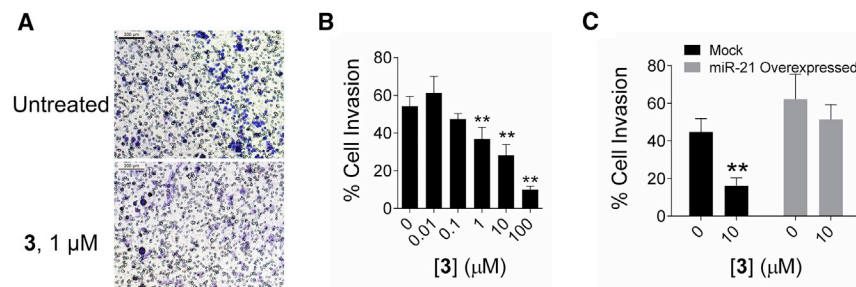


Figure 4. Evaluation of Phenotypic Effects of 3

(A) Representative images of reduced invasion observed in MDA-MB-231 cells after miR-21 inhibition through 3 treatment (1 μM). Cells allowed to invade through Matrigel basement membrane matrix for 16 hr at 37°C using a Boyden chamber assay. Cells that invaded the matrix were fixed with 1% paraformaldehyde and stained with 0.1% crystal violet for visualization. Scale bar, 200 μm.

(B) Quantification of cell invasion shown in (A) (two biological replicates, four fields of view).

(C) Effect on invasion upon treatment with 3 (10 μM) when pre-miR-21 is overexpressed via transfection of a miR-21 plasmid in MDA-MB-231 cells.

**p < 0.01, as determined by a two-tailed Student t test.

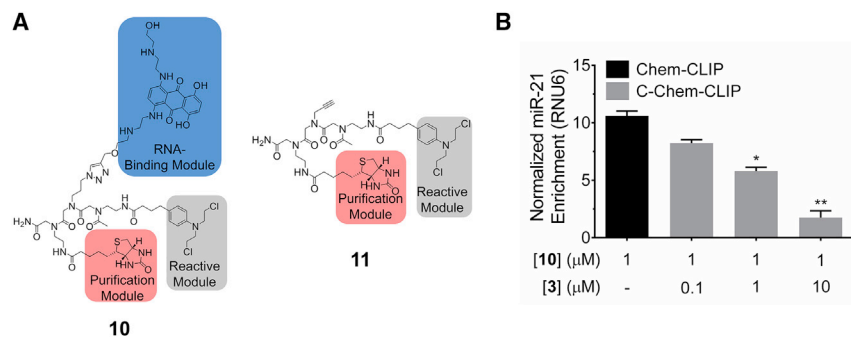


Figure 5. Chem-CLIP Target Validation Studies of 3 in MDA-MB-231 Cells

(A) Structures of **10**, 3-CA-Biotin, which is comprised of the RNA-binding module **3**, a biotin purification module and a crosslinking chlorambucil (CA) module, and control compound **11** (Control CA-Biotin), which lacks the RNA-binding module. (B) Chem-CLIP of pre-miR-21 using 1 μM of **10** in MDA-MB-231 cells and Competitive-Chem-CLIP (C-Chem-CLIP) of pre-miR-21 in MDA-MB-231 cells by using increasing concentrations of **3** to compete with **10** for binding (1 μM). * $p < 0.05$, ** $p < 0.01$, as determined by a two-tailed Student *t* test. Data represent means \pm SEM of biological triplicates.

See also Figure S5.

approach (Guan and Disney, 2013; Su et al., 2014). A Chem-CLIP probe was synthesized by appending a biotin and a chlorambucil crosslinking module onto **3** to afford compound **10** (Figure 5A). Compound **10** crosslinks with its cellular RNA targets, and the resulting small-molecule-RNA conjugates are harvested by biotin capture. Both *in vitro* and in cells, **10** reacted with pre-miR-21 (Figures 5B, S5A, and S5B). Importantly, co-addition of parent **3** and **10** in cells (competitive Chem-CLIP) decreased the extent of pull-down of pre-miR-21 in a dose-dependent manner (Figure 5B), thus proving that **3** binds its RNA target in cells. Chem-CLIP was also performed on **11** (Figure 5A), which lacks the RNA-binding module; no enrichment of miR-21 was observed in the pulled down fractions, whether *in vitro* or in cells, as expected (Figures S5A and S5C). Enrichment levels of miR-21 were normalized to levels of mature miR-21 after treatment with **10** or **11** (Figure S5D).

Selectivity of 3

The selectivity of **3** for inhibiting miR-21 was measured by using RT-qPCR, in particular by studying its effect on miRNAs that contain the same motifs in pre-miR-21's Dicer site, or RNA isoforms. Previous studies have identified that the expression levels of miRNAs will most likely be affected if the small molecule binds in a biologically important site, such as Dicer or Drosha processing sites (Velagapudi et al., 2014). Therefore, we queried a database of miRNA secondary structures to identify precursor miRNAs that contain the same A and/or U bulges found at or adjacent to pre-miR-21's Dicer processing sites (Figure 6A). Despite the presence of the A and/or U bulges in processing sites of other pre-miRNAs, only levels of miR-21 were affected (Figure 6B).

To determine if **3** does not inhibit levels of the other miRNAs studied because it does not bind the target in cells, we completed Chem-CLIP studies for the RNA isoforms (Figure 6C). Binding is observed to only two miRNAs, let-7e and miR-25; however, binding is not sufficient to reduce their mature levels. The binding site for **3** is located in the Dicer site of both pre-miRNAs (Liu et al., 2016); however, the lack of activity of **3** against let-7e and miR-25 could be traced to the fact that both let-7e and miR-25 are expressed at much lower levels compared with miR-21 (7% and 3%, respectively, compared with miR-21). Collectively, these results suggest that the enhanced anti-miR-21 activity of **3** is due to the presence of two binding sites in pre-miR-21

(only a singular binding site is present in pre-let-7e and pre-miR-25) and its comparatively much higher expression level.

DISCUSSION

This study has shown that various drug classes have the capacity to bind RNA, including topoisomerase inhibitors that affect a key non-coding, oncogenic miRNA. It has been suggested previously that topoisomerase II inhibitory activity that results in apoptosis in cancer cells (Swift et al., 2006). Thus, our studies may be another example of compounds whose activity can be traced to affecting multiple pathways. Other classes of small molecules have been shown to target RNA in addition to their previously known target. For example, the target of the antibacterial roseoflavin, the flavin mononucleotide riboswitch, was not uncovered until the discovery of riboswitches (Lee et al., 2009). Aggressive activity in re-purposing known drugs has revealed many additional targets across all types of biomolecules. It is likely that many drugs affect multiple pathways, some known and others unknown, to provide a therapeutic effect.

Extensive effort has been made to identify compounds that target miR-21 (Shortridge and Varani, 2015). Although several compounds have been shown to bind miR-21 *in vitro* (Connelly et al., 2017), only a few inhibit miR-21 levels in cells (Gumireddy et al., 2008; Naro et al., 2015; Shortridge et al., 2017). Most of the compounds identified were either transcriptional inhibitors or did not affect phenotype. Other studies showed that the aminoglycoside antibiotic streptomycin inhibited Dicer processing of pre-miR-21 and had a modest effect on apoptosis (about 25%) in MCF7 cells (Bose et al., 2012). As the RNA-targeting small molecule field emerges, careful consideration must be paid to the effect of compound on phenotype and its correlation with target modulation. In this study, it was found that **3** inhibited levels of mature miR-21, concomitantly increased levels of pre-miR-21, and reversed the invasive phenotype caused by elevated expression of miR-21 in triple-negative breast cancer cells. These effects are ablated upon overexpression of pre-miR-21, giving further support to **3**'s mechanism of action. An additional and important implication of these studies is that known drugs have potential to bind RNA. *In vitro* pharmacology studies on lead drug candidates only focuses at present on their liabilities to affect key proteins. Perhaps, additional studies should

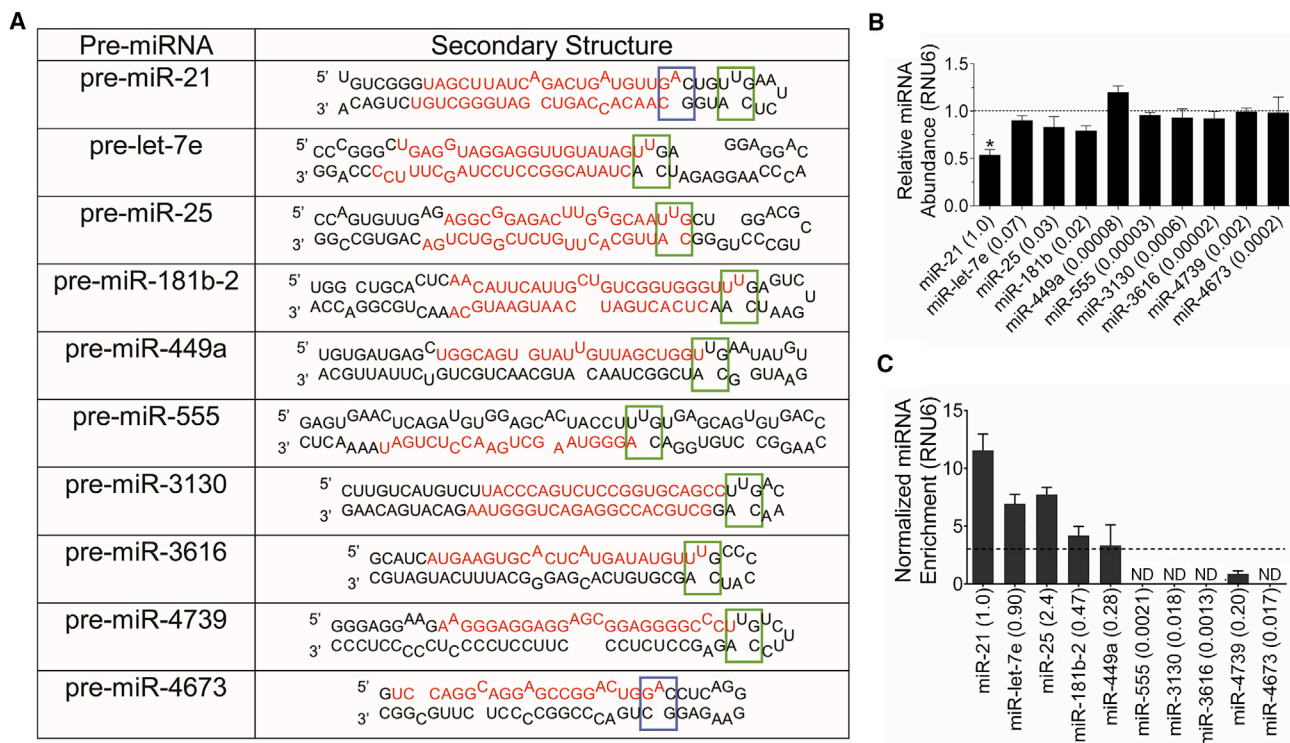


Figure 6. Selectivity Studies of 3

(A) Pre-miRNAs that contain the same A (blue box) and/or U bulge (green box) found in the Dicer site of pre-miR-21.

(B) Selectivity of **3** for miR-21 over other miRNAs with the same target A and/or U bulge, as determined by measuring mature miRNA levels by RT-qPCR. The numbers in parentheses after the miRNA name indicate relative expression levels as compared with miR-21.

(C) Pull-down of other miRNAs that contain A and/or U bulges by **10**. The numbers in parentheses after the miRNA name indicate relative expression level as compared with miR-21.

* $p < 0.05$ as determined by a two-tailed Student *t* test; ND indicates mature miRNA levels were not detectable ($C_t > 32$). Data represent means \pm SEM of biological triplicates.

be completed to understand the effect of lead molecules on the transcriptome as an additional safety screen.

The utility of these compounds to study miR-21 biology as chemical probes, however, is likely limited due to the multiple effects that the molecules have in cells. Other small molecules that have perhaps better selectivity are more useful chemical probes and include compounds targeting the ribosome and riboswitches (Carter et al., 2000; Poehlsgaard and Douthwaite, 2005).

Of further interest is the observation that kinase inhibitors are a key compound class that target RNA. These compounds have garnered much attention as clinical candidates, and many others are in pre-clinical development. It is also perhaps not surprising that these molecules target RNA given their penchant for having hydrogen bond donors and acceptors and the ability to stack with RNA bases. Thus, these molecules could be medicinally optimized to drug RNA and reach a clinical endpoint.

SIGNIFICANCE

Herein, we have developed a microarray-based method dubbed AbsorbArray to identify the preferred RNA motifs for unmodified small molecules. That is, the compounds do not require installation of a functional group for immobi-

lization. AbsorbArray was applied to the NIH Clinical Collection, a library of RNA-focused small molecules, RNA splicing modulators, and a library of kinase inhibitors. Indeed, these drugs, in particular topoisomerase inhibitors, kinase inhibitors, and RNA splicing modulators bind to RNAs. 2DCS and HiT-StARTS identified privileged motifs for each small molecule, and overlap was identified with oncogenic miR-21. One topoisomerase inhibitor, **3**, selectively inhibited miR-21 biogenesis, de-repressed a downstream protein, and reversed an invasive phenotype in MDA-MB-231 cells. These studies suggest that many known drugs have affinity for RNA, and that RNA may indeed be one of their cellular targets. Further, they lay the foundation for the rational repurposing of known drugs.

STAR METHODS

Detailed methods are provided in the online version of this paper and include the following:

- KEY RESOURCE TABLE
- EXPERIMENTAL MODEL AND SUBJECT DETAILS
- METHOD DETAILS

- General Nucleic Acids Methods
- Compound Libraries
- Construction of AbsorbArray-assisted Small Molecule Microarrays
- RNA Selection
- Reverse Transcription and PCR Amplification to Install Barcodes for RNA-Seq
- In Vitro Dicer Processing Assay
- RNA Isolation and RT-qPCR
- PTEN Luciferase Assay
- Imaging for DNA Damage
- Boyden Chamber Invasion Assay
- In Vitro Chem-CLIP and C-Chem-CLIP
- Cellular Chem-CLIP and C-Chem-CLIP
- In Vitro Topoisomerase Inhibition Assay
- Fluorescent Binding Affinity Measurements
- Microscale Thermophoresis (MST) Binding Measurements
- Chemical Synthesis
- QUANTIFICATION AND STATISTICAL ANALYSIS
- DATA AND SOFTWARE AVAILABILITY

SUPPLEMENTAL INFORMATION

Supplemental Information includes six figures and two tables and can be found with this article online at <https://doi.org/10.1016/j.chembiol.2018.05.015>.

ACKNOWLEDGMENTS

This work was funded by the Scheller Graduate Student Fellowship to M.G.C., a Swiss National Science Foundation Early Postdoc Mobility Fellowship to B.R.V., and the National Institutes of Health (5R01GM097455) to M.D.D.

AUTHOR CONTRIBUTIONS

M.D.D. directed the study, conceived of the ideas and designed experiments. S.P.V. designed and performed experiments. M.G.C. performed cellular experiments. T.T., B.R.V., Y.N., and H.S.H. performed 2DCS experiments. A.J.A. performed γ H2AX imaging for DNA damage. Y.M. made compounds **10** and **11**. A.K.C. provided RNA splicing modulator library. J.L.C.-D. performed *in vitro* Dicer experiment and wrote the paper, assisted by others. Z.F.W. performed MST binding assays.

DECLARATION OF INTERESTS

A patent application has been submitted on the Inforna software: Disney & Velagapudi, U.S. Patent Application 14/911,032.

Received: January 18, 2018

Revised: April 3, 2018

Accepted: May 18, 2018

Published: June 28, 2018

REFERENCES

Binaschi, M., Zunino, F., and Capranico, G. (1995). Mechanism of action of DNA topoisomerase inhibitors. *Stem Cells* **13**, 369–379.

Blount, K.F., and Breaker, R.R. (2006). Riboswitches as antibacterial drug targets. *Nat. Biotechnol.* **24**, 1558–1564.

Bose, D., Jayaraj, G., Suryawanshi, H., Agarwala, P., Pore, S.K., Banerjee, R., and Maiti, S. (2012). The tuberculosis drug streptomycin as a potential cancer therapeutic: inhibition of miR-21 function by directly targeting its precursor. *Angew. Chem. Int. Ed.* **51**, 1019–1023.

Calin, G.A., and Croce, C.M. (2006). MicroRNA-cancer connection: the beginning of a new tale. *Cancer Res.* **66**, 7390–7394.

Carter, A.P., Clemons, W.M., Brodersen, D.E., Morgan-Warren, R.J., Wimberly, B.T., and Ramakrishnan, V. (2000). Functional insights from the structure of the 30S ribosomal subunit and its interactions with antibiotics. *Nature* **407**, 340–348.

Chan, J.A., Krichevsky, A.M., and Kosik, K.S. (2005). MicroRNA-21 is an anti-apoptotic factor in human glioblastoma cells. *Cancer Res.* **65**, 6029–6033.

Childs-Disney, J.L., Wu, M., Pushechnikov, A., Aminova, O., and Disney, M.D. (2007). A small molecule microarray platform to select RNA internal loop-ligand interactions. *ACS Chem. Biol.* **2**, 745–754.

Childs-Disney, J.L., Yildirim, I., Park, H., Lohman, J.R., Guan, L., Tran, T., Sarkar, P., Schatz, G.C., and Disney, M.D. (2014). Structure of the myotonic dystrophy type 2 RNA and designed small molecules that reduce toxicity. *ACS Chem. Biol.* **9**, 538–550.

Chirayil, S., Wu, Q., Amezcua, C., and Luebke, K.J. (2014). NMR characterization of an oligonucleotide model of the miR-21 pre-element. *PLoS One* **9**, e108231.

Connelly, C.M., Boer, R.E., Moon, M.H., Gareiss, P., and Schneekloth, J.S., Jr. (2017). Discovery of inhibitors of microRNA-21 processing using small molecule microarrays. *ACS Chem. Biol.* **12**, 435–443.

Cooper, T.A., Wan, L., and Dreyfuss, G. (2009). RNA and disease. *Cell* **136**, 777–793.

Cserép, G.B., Baranyai, Z., Komáromy, D., Horváti, K., Bősze, S., and Kele, P. (2014). Fluorogenic tagging of peptides via Cys residues using thiol-specific vinyl sulfone affinity tags. *Tetrahedron* **70**, 5961–5965.

Dibrov, S.M., Parsons, J., Carnevali, M., Zhou, S., Rynearson, K.D., Ding, K., Garcia Segal, E., Brunn, N.D., Boerneke, M.A., Castaldi, M.P., et al. (2014). Hepatitis C virus translation inhibitors targeting the internal ribosomal entry site. *J. Med. Chem.* **57**, 1694–1707.

Disney, M.D., Labuda, L.P., Paul, D.J., Poplawski, S.G., Pushechnikov, A., Tran, T., Velagapudi, S.P., Wu, M., and Childs-Disney, J.L. (2008). Two-dimensional combinatorial screening identifies specific aminoglycoside-RNA internal loop partners. *J. Am. Chem. Soc.* **130**, 11185–11194.

ENCODE Project Consortium (2012). An integrated encyclopedia of DNA elements in the human genome. *Nature* **489**, 57–74.

Feofanov, A., Sharonov, S., Kudelina, I., Fleury, F., and Nabiev, I. (1997). Localization and molecular interactions of mitoxantrone within living K562 cells as probed by confocal spectral imaging analysis. *Biophys. J.* **73**, 3317–3327.

Frazier, K.S. (2015). Antisense oligonucleotide therapies: the promise and the challenges from a toxicologic pathologist's perspective. *Toxicol. Pathol.* **43**, 78–89.

Gareiss, P.C., Sobczak, K., McNaughton, B.R., Palde, P.B., Thornton, C.A., and Miller, B.L. (2008). Dynamic combinatorial selection of molecules capable of inhibiting the (CUG) repeat RNA-MBNL1 interaction *in vitro*: discovery of lead compounds targeting myotonic dystrophy (DM1). *J. Am. Chem. Soc.* **130**, 16254–16261.

Guan, L., and Disney, M.D. (2013). Covalent small molecule-RNA complex formation enables cellular profiling of small molecule-RNA interactions. *Angew. Chem. Int. Ed.* **52**, 10010–10013.

Gumireddy, K., Young, D.D., Xiong, X., Hogenesch, J.B., Huang, Q., and Deiters, A. (2008). Small molecule inhibitors of microRNA miR-21 function. *Angew. Chem. Int. Ed.* **47**, 7482–7484.

Hajihassan, Z., and Rabbani-Chadegani, A. (2011). The effect of mitoxantrone as an anticancer drug on hepatocytes nuclei and chromatin: selective release of histone proteins. *Indian J. Pharmacol.* **43**, 187–191.

Hampf, M., and Gossen, M. (2006). A protocol for combined Photinus and Renilla luciferase quantification compatible with protein assays. *Anal. Biochem.* **356**, 94–99.

Hergenrother, P.J., Depew, K.M., and Schreiber, S.L. (2000). Small-molecule microarrays: covalent attachment and screening of alcohol-containing small molecules on glass slides. *J. Am. Chem. Soc.* **122**, 7849–7850.

Huang, T.H., Wu, F., Loeb, G.B., Hsu, R., Heidersbach, A., Brincat, A., Horiuchi, D., Lebbink, R.J., Mo, Y.Y., Goga, A., et al. (2009). Up-regulation of

- miR-21 by HER2/neu signaling promotes cell invasion. *J. Biol. Chem.* **284**, 18515–18524.
- Ivanov, A.I., Christodoulou, J., Parkinson, J.A., Barnham, K.J., Tucker, A., Woodrow, J., and Sadler, P.J. (1998). Cisplatin binding sites on human albumin. *J. Biol. Chem.* **273**, 14721–14730.
- Jahromi, A.H., Nguyen, L., Fu, Y., Miller, K.A., Baranger, A.M., and Zimmerman, S.C. (2013). A novel CUG^{exp}-MBNL1 inhibitor with therapeutic potential for myotonic dystrophy type 1. *ACS Chem. Biol.* **8**, 1037–1043.
- Kumar, A., Parkesh, R., Sznajder, L.J., Childs-Disney, J.L., Sobczak, K., and Disney, M.D. (2012). Chemical correction of pre-mRNA splicing defects associated with sequestration of muscleblind-like 1 protein by expanded r(CAG)-containing transcripts. *ACS Chem. Biol.* **7**, 496–505.
- Lee, E.R., Blount, K.F., and Breaker, R.R. (2009). Roseoflavin is a natural antibacterial compound that binds to FMN riboswitches and regulates gene expression. *RNA Biol.* **6**, 187–194.
- Lee, M.K., Bottini, A., Kim, M., Bardaro, M.F., Jr., Zhang, Z., Pellecchia, M., Choi, B.S., and Varani, G. (2014). A novel small-molecule binds to the influenza A virus RNA promoter and inhibits viral replication. *Chem. Commun. (Camb.)* **50**, 368–370.
- Li, J., Yen, C., Liaw, D., Podsypanina, K., Bose, S., Wang, S.I., Puc, J., Miliareis, C., Rodgers, L., McCombie, R., et al. (1997). PTEN, a putative protein tyrosine phosphatase gene mutated in human brain, breast, and prostate cancer. *Science* **275**, 1943–1947.
- Liang, X.-h., Sun, H., Shen, W., and Crooke, S.T. (2015). Identification and characterization of intracellular proteins that bind oligonucleotides with phosphorothioate linkages. *Nucleic Acids Res.* **43**, 2927–2945.
- Liu, Y., Peacey, E., Dickson, J., Donahue, C.P., Zheng, S., Varani, G., and Wolfe, M.S. (2009). Mitoxantrone analogues as ligands for a stem-loop structure of tau pre-mRNA. *J. Med. Chem.* **52**, 6523–6526.
- Liu, B., Childs-Disney, J.L., Znosko, B.M., Wang, D., Fallahi, M., Gallo, S.M., and Disney, M.D. (2016). Analysis of secondary structural elements in human microRNA hairpin precursors. *BMC Bioinformatics* **17**, 112.
- Lown, J.W., Hanstock, C.C., Bradley, R.D., and Scraba, D.G. (1984). Interactions of the antitumor agents mitoxantrone and bisantrene with deoxyribonucleic acids studied by electron microscopy. *Mol. Pharmacol.* **25**, 178–184.
- MacBeath, G., and Schreiber, S.L. (2000). Printing proteins as microarrays for high-throughput function determination. *Science* **289**, 1760–1763.
- MacBeath, G., Koehler, A.N., and Schreiber, S.L. (1999). Printing small molecules as microarrays and detecting protein-ligand interactions en masse. *J. Am. Chem. Soc.* **121**, 7967–7968.
- Mansour, O.C., Evison, B.J., Sleebs, B.E., Watson, K.G., Nudelman, A., Rephaeli, A., Buck, D.P., Collins, J.G., Bilardi, R.A., Phillips, D.R., et al. (2010). New anthracenedione derivatives with improved biological activity by virtue of stable drug-DNA adduct formation. *J. Med. Chem.* **53**, 6851–6866.
- Marcheschi, R.J., Mouzakis, K.D., and Butcher, S.E. (2009). Selection and characterization of small molecules that bind the HIV-1 frameshift site RNA. *ACS Chem. Biol.* **4**, 844–854.
- McConnell, A.J., Serpell, C.J., Thompson, A.L., Allan, D.R., and Beer, P.D. (2010). Calix[4]arene-based rotaxane host systems for anion recognition. *Chemistry* **16**, 1256–1264.
- Mei, H.-Y., Galan, A.A., Halim, N.S., Mack, D.P., Moreland, D.W., Sanders, K.B., Hoa, N.T., and Czarnik, A.W. (1995). Inhibition of an HIV-1 Tat-derived peptide binding to TAR RNA by aminoglycoside antibiotics. *Bioorg. Med. Chem. Lett.* **5**, 2755–2760.
- Meng, F., Henson, R., Wehbe-Janek, H., Ghoshal, K., Jacob, S.T., and Patel, T. (2007). MicroRNA-21 regulates expression of the PTEN tumor suppressor gene in human hepatocellular cancer. *Gastroenterology* **133**, 647–658.
- Moon, M.H., Hilimire, T.A., Sanders, A.M., and Schneekloth, J.S., Jr. (2018). Measuring RNA-ligand interactions with microscale thermophoresis. *Biochemistry*. <https://doi.org/10.1021/acs.biochem.7b01141>.
- Morrow, T. (2017). New therapy for spinal muscular atrophy offers modest bang for pharmaceutical buck. *Manag. Care* **26**, 36–37.
- Naro, Y., Thomas, M., Stephens, M.D., Connelly, C.M., and Deiters, A. (2015). Aryl amide small-molecule inhibitors of microRNA miR-21 function. *Bioorg. Med. Chem. Lett.* **25**, 4793–4796.
- Naryshkin, N.A., Weetall, M., Dakka, A., Narasimhan, J., Zhao, X., Feng, Z., Ling, K.K., Karp, G.M., Qi, H., Woll, M.G., et al. (2014). Motor neuron disease. SMN2 splicing modifiers improve motor function and longevity in mice with spinal muscular atrophy. *Science* **345**, 688–693.
- O'Donnell, K.A., Wentzel, E.A., Zeller, K.I., Dang, C.V., and Mendell, J.T. (2005). c-Myc-regulated microRNAs modulate E2F1 expression. *Nature* **435**, 839–843.
- Palacino, J., Swalley, S.E., Song, C., Cheung, A.K., Shu, L., Zhang, X., Van Hoosear, M., Shin, Y., Chin, D.N., Keller, C.G., et al. (2015). SMN2 splice modulators enhance U1-pre-mRNA association and rescue SMA mice. *Nat. Chem. Biol.* **11**, 511–517.
- Panwar, B., Omenn, G.S., and Guan, Y. (2017). miRmine: a database of human miRNA expression profiles. *Bioinformatics* **33**, 1554–1560.
- Pilch, D.R., Sedelnikova, O.A., Redon, C., Celeste, A., Nussenzweig, A., and Bonner, W.M. (2003). Characteristics of γ -H2AX foci at DNA double-strand breaks sites. *Biochem. Cell Biol.* **81**, 123–129.
- Poehlsgaard, J., and Douthwaite, S. (2005). The bacterial ribosome as a target for antibiotics. *Nat. Rev. Microbiol.* **3**, 870–881.
- Pushechnikov, A., Lee, M.M., Childs-Disney, J.L., Sobczak, K., French, J.M., Thornton, C.A., and Disney, M.D. (2009). Rational design of ligands targeting triplet repeating transcripts that cause RNA dominant disease: application to myotonic muscular dystrophy type 1 and spinocerebellar ataxia type 3. *J. Am. Chem. Soc.* **131**, 9767–9779.
- du Rieu, M.C., Torrisani, J., Selves, J., Al Saati, T., Souque, A., Dufresne, M., Tsongalis, G.J., Suriawinata, A.A., Carrere, N., Buscail, L., et al. (2010). MicroRNA-21 is induced early in pancreatic ductal adenocarcinoma precursor lesions. *Clin. Chem.* **56**, 603–612.
- Rogakou, E.P., Boon, C., Redon, C., and Bonner, W.M. (1999). Megabase chromatin domains involved in DNA double-strand breaks in vivo. *J. Cell Biol.* **146**, 905–916.
- Rzuczek, S.G., Southern, M.R., and Disney, M.D. (2015). Studying a drug-like, RNA-focused small molecule library identifies compounds that inhibit RNA toxicity in myotonic dystrophy. *ACS Chem. Biol.* **10**, 2706–2715.
- Rzuczek, S.G., Colgan, L.A., Nakai, Y., Cameron, M.D., Furling, D., Yasuda, R., and Disney, M.D. (2017). Precise small-molecule recognition of a toxic CUG RNA repeat expansion. *Nat. Chem. Biol.* **13**, 188–193.
- Seidel, S.A.I., Dijkman, P.M., Lea, W.A., van den Bogaart, G., Jerabek-Willemsen, M., Lazić, A., Joseph, J.S., Srinivasan, P., Baaske, P., Simeonov, A., et al. (2013). Microscale thermophoresis quantifies biomolecular interactions under previously challenging conditions. *Methods* **59**, 301–315.
- Seike, M., Goto, A., Okano, T., Bowman, E.D., Schetter, A.J., Horikawa, I., Mathe, E.A., Jen, J., Yang, P., Sugimura, H., et al. (2009). MiR-21 is an EGFR-regulated anti-apoptotic factor in lung cancer in never-smokers. *Proc. Natl. Acad. Sci. USA* **106**, 12085–12090.
- Shaul, P., Frenkel, M., Goldstein, E.B., Mittelman, L., Grunwald, A., Ebenstein, Y., Tsarfaty, I., and Fridman, M. (2013). The structure of anthracycline derivatives determines their subcellular localization and cytotoxic activity. *ACS Med. Chem. Lett.* **4**, 323–328.
- Shortridge, M.D., and Varani, G. (2015). Structure based approaches for targeting non-coding RNAs with small molecules. *Curr. Opin. Struct. Biol.* **30**, 79–88.
- Shortridge, M.D., Walker, M.J., Pavelitz, T., Chen, Y., Yang, W., and Varani, G. (2017). A macrocyclic peptide ligand binds the oncogenic microRNA-21 precursor and suppresses dicer processing. *ACS Chem. Biol.* **12**, 1611–1620.
- Su, Z., Zhang, Y., Gendron, T.F., Bauer, P.O., Chew, J., Yang, W.Y., Fostvedt, E., Jansen-West, K., Belzil, V.V., Desaro, P., et al. (2014). Discovery of a biomarker and lead small molecules to target r(GGGGCC)-associated defects in c9FTD/ALS. *Neuron* **84**, 239.
- Swift, L.P., Rephaeli, A., Nudelman, A., Phillips, D.R., and Cutts, S.M. (2006). Doxorubicin-DNA adducts induce a non-topoisomerase II-mediated form of cell death. *Cancer Res.* **66**, 4863–4871.

- Tenson, T., and Mankin, A. (2006). Antibiotics and the ribosome. *Mol. Microbiol.* **59**, 1664–1677.
- Velagapudi, S.P., Gallo, S.M., and Disney, M.D. (2014). Sequence-based design of bioactive small molecules that target precursor microRNAs. *Nat. Chem. Biol.* **10**, 291–297.
- Velagapudi, S.P., Luo, Y., Tran, T., Haniff, H.S., Nakai, Y., Fallahi, M., Martinez, G.J., Childs-Disney, J.L., and Disney, M.D. (2017). Defining RNA-small molecule affinity landscapes enables design of a small molecule inhibitor of an oncogenic noncoding RNA. *ACS Cent. Sci.* **3**, 205–216.
- Volinia, S., Calin, G.A., Liu, C.G., Ambs, S., Cimmino, A., Petrocca, F., Visone, R., Iorio, M., Roldo, C., Ferracin, M., et al. (2006). A microRNA expression signature of human solid tumors defines cancer gene targets. *Proc. Natl. Acad. Sci. USA* **103**, 2257–2261.
- Yan, L.X., Huang, X.F., Shao, Q., Huang, M.Y., Deng, L., Wu, Q.L., Zeng, Y.X., and Shao, J.Y. (2008). MicroRNA miR-21 overexpression in human breast cancer is associated with advanced clinical stage, lymph node metastasis and patient poor prognosis. *RNA* **14**, 2348–2360.
- Yang, W.Y., Wilson, H.D., Velagapudi, S.P., and Disney, M.D. (2015). Inhibition of non-ATG translational events in cells via covalent small molecules targeting RNA. *J. Am. Chem. Soc.* **137**, 5336–5345.
- Yang, W.Y., He, F., Strack, R.L., Oh, S.Y., Frazer, M., Jaffrey, S.R., Todd, P.K., and Disney, M.D. (2016). Small molecule recognition and tools to study modulation of r(CG)(exp) in fragile X-associated tremor ataxia syndrome. *ACS Chem. Biol.* **11**, 2456–2465.
- Zapp, M.L., Stern, S., and Green, M.R. (1993). Small molecules that selectively block RNA binding of HIV-1 Rev protein inhibit Rev function and viral production. *Cell* **74**, 969–978.
- Zheng, S., Chen, Y., Donahue, C.P., Wolfe, M.S., and Varani, G. (2009). Structural basis for stabilization of the Tau pre-mRNA splicing regulatory element by novantrone (mitoxantrone). *Chem. Biol.* **16**, 557–566.
- Zhu, S., Wu, H., Wu, F., Nie, D., Sheng, S., and Mo, Y.Y. (2008). MicroRNA-21 targets tumor suppressor genes in invasion and metastasis. *Cell Res.* **18**, 350–359.

STAR★METHODS

KEY RESOURCE TABLE

REAGENT or RESOURCE	SOURCE	IDENTIFIER
Antibodies		
anti-phospho-Histone-H2A.X (Ser139)	EMD Millipore	clone JBW301; RRID: AB_568825
Goat anti-Mouse IgG Secondary Antibody, DyLight 488	Thermo Fisher	Catalog #:35502; RRID: AB_844397
Chemicals, Peptides, and Recombinant Proteins		
1	Cayman Chemicals	Catalog# 15007
2	Biotang, Inc.	Catalog# RS023
3	Biotang, Inc.	Catalog# RM11
NIH Clinical Collection (NIH-CC)	Scripps Molecular Screening Center	NA
SYNLibrary-95	Synkinase	Catalog# SYN-2103
pre-mRNA splicing regulators	California Institute for Biomedical Research	N/A
RNA-focused compound library	Scripps Molecular Screening Center	N/A
Critical Commercial Assays		
Topoisomerase II Drug Screening Kit	TopoGEN, Inc.	Catalog# TG1009
Oligonucleotides		
Primers used for RT-qPCR, see Table S2	This paper	N/A
hsa-miR-21-5p, miRCURY LNA Power microRNA inhibitor	Exiqon (now a part of Qiagen)	Catalog# 4100689-101
Negative control A, miRCURY LNA Power microRNA inhibitor control	Exiqon (now a part of Qiagen)	Catalog# 199006-102
Recombinant DNA		
pGL3-PTEN-3'UTR	Addgene	Plasmid # 21326
pcDNA3-miR21	Addgene	Plasmid # 21114
pRL Renilla Luciferase Control	Promega	Plasmid # E223A
Software and Algorithms		
Olympus Fluoview software version 3.0	Olympus	N/A
QuantityOne	BioRad	N/A
Graphpad Prism 7	GraphPad Prism Software, Inc.	N/A
Inforna	Disney Laboratory	https://disney.florida.scripps.edu/software/

EXPERIMENTAL MODEL AND SUBJECT DETAILS

All cells were grown at 37°C and 5% CO₂. MDA-MB-231 (ATCC: HTB-26) cells were cultured in Roswell Park Memorial Institute (RPMI) 1640 medium supplemented with 1% penicillin/streptomycin, 1% glutagro (Corning) and 10% fetal bovine serum (FBS) (complete growth medium). Cells were directly purchased from ATCC but were not authenticated.

METHOD DETAILS

General Nucleic Acids Methods

All DNA oligonucleotides were purchased from Integrated DNA Technologies, Inc. (IDT) and used without further purification. The RNA competitor oligonucleotides and pre-miR-21 constructs for MST were purchased from Dharmacon and de-protected according to the manufacturer's standard procedure. Competitor oligonucleotides were used to ensure that RNA-small molecule interactions were confined to the randomized region of 3×2 nucleotide internal loop pattern). All aqueous solutions were made with nanopure water. The RNA library was transcribed by *in vitro* transcription from the corresponding DNA template.

Compound Libraries

The 727-member NIH Clinical Collection (NIH-CC) was obtained from Scripps Molecular Screening Center. The NIH-CC is a small molecule library comprised of drugs that have been in Phase I or II clinical trials. Thus, compounds were selected for drug-likeness, bioavailability, and stability. The 95-member Kinase library (SYNLibrary-95, catalog # SYN-2103) was purchased from Synkinase. SYNLibrary-95 contains a kinase inhibitor library that recognizes 57 targets. Three pre-mRNA splicing regulators were obtained from the California Institute for Biomedical Research (Calibr). The 201-member RNA-focused compound library was obtained from Scripps Molecular Screening Center. These compounds were previously identified by performing chemical similarity search based on molecules that possess *bis*-benzimidazole or similar cores (Rzuczek et al., 2015). Hit compounds were re-purchased in larger quantities for testing. Compound **1** was purchased from Cayman Chemicals, while **2** and **3** were purchased from Biotang, Inc.

Construction of AbsorbArray-assisted Small Molecule Microarrays

Microarrays were constructed by pouring 15 mL of 1% molten agarose solution onto a glass slide [85.5 x 127.8 x 1.1 mm width x height x thickness]. The agarose was then air dried for 1 h at room temperature to form a thick gel surface. A 200 nL aliquot of compound (10 mM in DMSO) was then pinned into the agarose gel from a 384-well plate (Greiner; catalog #781201-906) using a Biomek NX^P Laboratory Automation Workstation equipped with a 100 nL 384-pin floating head with diameter 0.787 mm and inter-pin distance of 4.5 mm. The compound-spotted slides were allowed to air dry completely to form a thin, invisible agarose layer. After drying, slides were washed three times with 1 x PBST (1 x PBS+0.1% Tween) followed by washing three times for 5 min with nanopure water and air dried completely. 2DCS of the final hit compounds were completed on microscopic slides [Fisher Scientific, 12550016; 75 x 25 x 1 mm (width x height x thickness); see Figure S1]. Quantification of compound spotting before and after washing was analyzed using QuantityOne software (BioRad).

RNA Selection

2DCS selections were completed as previously described (Disney et al., 2008). All oligonucleotides, including 5'-end ³²P-labeled RNA library [prepared as described previously (Disney et al., 2008)], competitor chase oligonucleotides (Figure 2D) and tRNA, were folded separately in 1 x Hybridization Buffer (HB, 8 mM Na₂HPO₄, pH 7.0, 185 mM NaCl, and 1 mM EDTA) by heating at 90°C for 2 min followed by cooling to room temperature on the bench top. The 5'-end ³²P-labeled folded RNAs (~50,000 counts by Geiger counter) were mixed together and MgCl₂ and bovine serum albumin (BSA) were added at 1 mM and 40 μg/mL final concentrations, respectively, in a total volume of 3000 μL. Prior to hybridization, microarrays were pre-equilibrated with 3000 μL of 1 x HB supplemented with 1 mM MgCl₂ and 40 μg/mL BSA (1 x HB2) for 10 min at room temperature to prevent non-specific binding. After the slides were pre-equilibrated, HB2 was removed and the mixture of folded RNAs was applied to the microarray surface and distributed evenly across the array surface with a custom-cut piece of Parafilm (solution height ~2-3 mm). The slide was hybridized for approximately 45 min at room temperature. After incubation, the Parafilm was removed, and the slide was washed by submersion in 30 mL of HB for 5 s with gentle agitation three times. Excess buffer was removed completely from the slide, and the slide was dried at room temperature for 30 min. While compounds may diffuse from their initial spot, significant interspot diffusion of the RNA-ligand complexes was not observed. Although diffusion rates differ depending on the physical/chemical properties of each compound, washing of the plates before and after hybridization will remove complexes that have diffused out of the spotted area. The microarray was exposed to a phosphorimager screen and imaged using a Molecular Devices Typhoon phosphorimager. The resulting image was used as a template to harvest bound RNAs from the microarray surface. To harvest bound RNAs, 1 μL of nanopure water was added to each spot. After 30 s, the buffer was absorbed and the agarose gel at that spot was excised using a toothpick.

Reverse Transcription and PCR Amplification to Install Barcodes for RNA-Seq

The excised agarose was placed into a thin-walled PCR tube with 18 μL of water, 2 μL of 10x RQ1 DNase I buffer and 2 units of RQ1 RNase-free DNase (Promega). The solution was incubated at 37°C for 2 h and then quenched by addition of 2 μL of 10x DNase stop solution (Promega). Samples were incubated at 65°C for 10 min to completely inactivate the DNase and then subjected to RT-PCR amplification to install a unique barcode. Reverse transcription reactions were completed in 1 x RT buffer, 1 mM dNTPs, 5 μM RT primer (5'-CCTCTCTATGGGCAGTCGGTGATCCTTGCGG ATCCAAT), 200 μg/mL BSA, 4 units of AMV reverse transcriptase, and 20 μL of DNase-treated selected RNAs. Samples were incubated at 60°C for 1 h. A 20 μL aliquot of the RT reaction was added to 6 μL of 10x PCR Buffer, 4 μL of 100 μM forward primer including barcode (5'-CCATCTC ATCCCTGCGTGTCTCCGACTCAG-XXXXXXXXXXGATGGGAGAGGGTTTAAT where X represents unique barcode, GAT is the barcode adapter), 2 μL of 100 μM reverse primer, 0.6 μL of 250 mM MgCl₂, and 2 μL of Taq DNA polymerase. Two-step PCR was performed at 95°C for 1 min and 72°C for 1 min. Aliquots of the RT-PCR product were checked every two cycles starting at cycle 10 on a non-denaturing 8% polyacrylamide gel stained with SYBR Green to ensure that background spots (excised from the array where compound was not delivered) were not amplified. RT-PCR products encoding selected RNAs were purified on a non-denaturing 8% polyacrylamide gel. Purity was assessed using a Bioanalyzer and samples were mixed in equal amounts and sequenced using an Ion Proton deep sequencer using PI chips (60-80 million reads).

In Vitro Dicer Processing Assay

The miR-21 precursor (pre-miR-21) was 5'-end labeled with [γ - 32 P] ATP and T4 polynucleotide kinase as previously described (Velagapudi et al., 2014). The RNA was then folded in 1× Reaction Buffer (Genlantis) by heating at 60°C for 5 min and slowly cooling to room temperature, where it was then supplemented with 1 mM ATP and 2.5 mM MgCl₂. Compound was added to the reaction mixture and the samples were allowed to incubate at room temperature for 15 min. Recombinant human Dicer enzyme (Genlantis) was added to a final concentration of 0.01 U/ μ L and the samples were incubated for an additional 30 min at 37°C. Reactions were stopped by adding in 2× Gel Loading Buffer (8 M urea, 50 mM EDTA, 0.05% (w/v) bromophenol blue, 0.05% (w/v) xylene cyanol). To generate sequencing markers, pre-miR-21 was digested with RNase T1 (0.125 U/ μ L) in T1 Buffer (25 mM sodium citrate, pH 5, 7 M urea, and 1 mM EDTA) for 20 min at room temperature. An RNA hydrolysis ladder was prepared by incubating RNA in 1× RNA Hydrolysis Buffer (50 mM NaHCO₃, 1 mM EDTA, pH 9.4) at 95°C for 5 min. Cleavage products were resolved on a denaturing 15% polyacrylamide gel, which was imaged using a Molecular Dynamics Typhoon phosphorimager and quantified with Bio-Rad's QuantityOne software.

RNA Isolation and RT-qPCR

MDA-MB-231 cells were cultured as described above and grown to 80% confluency in 24-well plates. Cells were treated with compound of interest for 24-48 h. Total RNA was then extracted with a Quick-RNA MiniPrep Kit (Zymo Research) per the manufacturer's protocol. Approximately 200 ng of total RNA was used for reverse transcription reactions (RT), which were completed by using a miScript II RT Kit (Qiagen) per the manufacturer's protocol. RT-qPCR was completed using a 7900HT Fast Real Time PCR System (Applied Biosystems), using Power SYBR Green Master Mix (Life Technologies). Primers for RT-qPCR were purchased from IDT or Eurofins (see Table S2) and used without further purification. Expression levels of RNAs were normalized to U6 small nuclear RNA or 18S rRNA.

PTEN Luciferase Assay

MDA-MB-231 cells were grown in 48-well plates to ~60% confluency in complete growth medium. The cells were transiently co-transfected with 200 ng of a plasmid encoding the 3' untranslated region (UTR) of PTEN fused to luciferase (O'Donnell et al., 2005) and 40 ng of a plasmid encoding Renilla luciferase using Lipofectamine 2000 per the manufacturer's protocol. At 5 h post-transfection, compounds were added in complete growth medium, and the cells were incubated for 48 h. Luciferase assays were completed based on a previously described protocol (Hampf and Gossen, 2006). Cells were lysed in 40 μ L 1× Lysis Buffer (100 mM potassium phosphate buffer, pH 7.8, 0.2% Tween 20) for 10 min at room temperature. Next, 150 μ L of 1× Firefly Luciferase Buffer (200 mM Tris-HCl, pH 8, 15 mM magnesium sulfate, 0.1 mM EDTA, 25 mM dithiothreitol, 1 mM ATP, 200 μ M coenzyme A, and 200 μ M luciferin) and incubated for 2 min at room temperature. Luminescence signal was measured on a Biotek Flx800 plate reader. To measure Renilla luciferase activity, 150 μ L of 1× Renilla Luciferase Buffer (25 mM sodium pyrophosphate, 10 mM sodium acetate, 15 mM EDTA, 500 mM sodium sulfate, 500 mM sodium chloride, 50 μ M of 4-(6-Methyl-2-benzothiazolyl)benzeneamine (CAS# 92-36-4), and 4 μ M benzyl-coelenterazine, pH 5.0) was added and incubated for 2 min at room temperature. Luminescence signal was measured on a Biotek Flx800 plate reader.

Imaging for DNA Damage

The γ -H2AX immunofluorescence assay was used to assess DNA double strand breaks in cells (Pilch et al., 2003; Rogakou et al., 1999). MDA-MB-231 cells were grown to ~80% confluence in a Mat-Tek 96-well glass bottom plate in growth medium. Cells were treated with **3** in complete growth medium for 24 hr. Cells were washed with 1× DPBS then fixed with 4% paraformaldehyde in 1× DPBS at 37°C and 5% CO₂ for 10 min. Cells were washed 5 times with 1× DPBS and three times with 0.1% Triton X-100 in 1× DPBS for 5 min at 37°C and 5% CO₂. Cells were then washed with 30% formamide in 2× SSC buffer for 10 min at room temperature and 2× SSC for 30 min at 37°C and 5% CO₂. Cells were incubated with a 1:500 dilution of anti-phospho-Histone-H2A.X (Ser139) (clone JBW301, EMD Millipore) in 2× SSC for 1 h at 37°C and 5% CO₂ then washed three times with 0.1% Triton X-100 in 1× DPBS for 5 min at 37°C and 5% CO₂. Cells were incubated with a 1:200 dilution of goat anti-mouse IgG-DyLight 488 conjugate (Thermo Fisher) in 2× SSC for 1 h at 37°C and 5% CO₂ and then washed three times with 0.1% Triton X-100 in 1× DPBS for 5 min at 37°C and 5% CO₂. Cells were washed three times with 1× DPBS and then stained using a 1 μ g/ μ L solution of DAPI in 1× DPBS for 5 min at 37°C and 5% CO₂. Cells were washed five times in 1× DPBS and then imaged in 1× DPBS using an Olympus Fluoview 1000 confocal microscope at 40× magnification. Anti- γ -H2AX fluorescence intensity was quantified using Olympus Fluoview software version 3.0. Average Anti- γ -H2AX fluorescence intensity measurements represent the average fluorescence intensity across eight images.

Boyden Chamber Invasion Assay

Matrigel (Corning) was thawed overnight at 4°C., diluted to 3 mg/mL of basement protein, and then dispensed into 24 well tissue culture inserts with 8 μ m pore sizes (100 L; μ Greiner). The inserts containing Matrigel were incubated at 37°C for 15 min and then placed back into 4°C overnight. The following day, 50000 MDA-MB-231 cells in growth medium lacking FBS with or without **3** were added to the inserts and allowed to migrate towards complete growth medium in the bottom wells for 16 h. The medium

was vacuum aspirated from both hanging cell culture inserts and bottom wells, which were then washed twice with 1 × PBS with gentle shaking. Excess liquid and non-invading cells inside the insert were removed with cotton swabs. 400 μL of 4% paraformaldehyde in 1 × PBS was added to bottom wells and incubated for 20 min at room temperature. The wells and inserts were then washed twice with 1 × PBS and treated with 400 μL of 0.1% crystal violet solution in 1 × PBS for 20 min at room temperature. After staining, the wells and inserts were washed twice with water, once with 1 × PBS, and then dried with cotton swabs. After air-drying, the inserts were analyzed by microscopy using a Leica DMI3000 B upright fluorescent microscope. Invading cells from four different fields of view from each captured image were counted. Alternatively, MDA-MB-231 cells were transfected with a plasmid containing pre-miR-21 (Addgene) using Lipofectamine 2000 according to the manufacturer's protocol, and the experiment was performed as described above.

In Vitro Chem-CLIP and C-Chem-CLIP

Approximately 50000 counts of ³²P 5'-end labeled pre-miR-21 were added to inactivated DMEM growth medium and folded at 95°C for 45 s, then cooled on ice for 5 min. Compound **10** or **11** was added to the folded RNA and incubated at 37°C overnight. For C-Chem-CLIP, nucleic acids were pre-treated with dilutions of **3** for 15 min at room temperature before Chem-CLIP probes were added. Streptavidin-agarose beads (Sigma-Aldrich, S1638; ≥15 μg/mL binding capacity) were washed three times with 1 × PBS and resuspended in 1 × PBS. Beads were added to the samples and incubated for 1 h at room temperature. Samples were centrifuged and the supernatant was transferred to a new tube. Beads were washed three times with 1 × PBS with 0.1% (v/v) Tween-20 and centrifuged, with each wash being added to the supernatant tube. Radioactivity in the beads and the supernatant/wash tubes were quantified using a Beckman Coulter LS6500 Liquid Scintillation Counter.

Cellular Chem-CLIP and C-Chem-CLIP

MDA-MB-231 cells were grown to ~70% confluency as monolayers in 100 mm dishes and treated with 1 μM of **10** or **11** for 8 h. Total RNA was extracted using a Quick-RNA MiniPrep Kit (Zymo Research) per the manufacturer's protocol. Approximately 30 μg of total RNA was then incubated with 100 μL of streptavidin-agarose beads (Sigma-Aldrich) and shaken for 1 h at room temperature. The solution was removed and beads washed six times with 300 μL of 1 × PBS. The RNA bound to beads was released by heating at 65°C for 20 min in 1 × Elution Buffer (95% formamide, 10 mM EDTA, pH 8.2). Eluted RNA was then purified with a Quick-RNA MiniPrep Kit (Zymo Research) and used for subsequent RT-qPCR analysis as described above.

Normalized miRNA Enrichment of the measured RNA before and after pulldown was measured using Equation 1:

$$\text{Normalized miRNA Enrichment} : 2^{-(\Delta C_t \text{ before pulldown} - \Delta C_t \text{ after pulldown})} \quad (\text{Equation 1})$$

where “ ΔC_t before pulldown” is the difference between the C_t values for the RNA of interest and a housekeeping gene (U6 small nuclear RNA) in total RNA isolated from cell lysate RNA (no pulldown) and “ ΔC_t after pulldown” is the difference between the C_t values for the RNA of interest and the same housekeeping gene after pulldown. Data were normalized to the levels of mature miR-21 measured after treatment with Chem-CLIP probe at the appropriate concentration.

In Vitro Topoisomerase Inhibition Assay

Topoisomerase II inhibitory activity was measured using a Topoisomerase II Drug Screening Kit (TopoGEN, Inc.) per the manufacturer's protocol. Dilutions of **1**, **2**, and **3** in water were added to 300 ng of DNA in 1 × Complete Buffer (50 mM Tris-HCl, pH 8, 150 mM NaCl, 10 mM MgCl₂, 0.5 mM dithiothreitol, 30 μg/mL BSA, and 2 mM ATP), followed by addition of 7.5 U of Topoisomerase II enzyme. Samples were incubated at 37°C for 30 min, and the reaction was stopped by adding 2 μL of 10% sodium dodecyl sulfate (SDS). Proteinase K (50 μg/mL) was added, and the samples were incubated at 37°C for 15 min. Topoisomers were separated on 1% agarose gels with or without 0.5 μg/mL ethidium bromide. Gels prepared with ethidium bromide were run in 1 × TAE running buffer supplemented with 0.5 μg/mL ethidium bromide. Gels run without ethidium bromide were post stained with 0.5 μg/mL ethidium bromide. Both gels were destained in 1 × TAE for 15 min and DNA products were visualized using a Bio-Rad Gel Doc XR+ imaging system (Figure S4).

Fluorescent Binding Affinity Measurements

Dissociation constants were determined using an in-solution fluorescence-based assay. The RNA of interest was folded in 1 × Assay Buffer (8 mM Na₂HPO₄, pH 7.0, 190 mM NaCl, 1 mM EDTA and 40 μg/mL BSA) by heating at 60°C for 5 min and slowly cooling to room temperature. Small molecules were added to a final concentration of 250 nM for **3**, or 2000 nM for **1** and **2**. Serial dilutions (1:2) were then completed in 1 × Assay Buffer supplemented with 250 nM of **3**, or 2000 nM of **1** and **2**. The solutions were incubated for 30 min at room temperature and then transferred to a 96-well plate and fluorescence intensity was measured. The change in fluorescence intensity as a function of RNA concentration was fit to Equation 2:

$$f(x) = B_{\max} \times \left(\frac{[RNA]^h}{K_d^h + [RNA]^h} \right) \quad \text{Equation (2)}$$

where B_{\max} , is maximum specific binding; $[RNA]$, is RNA concentration; h , is Hill slope.

Microscale Thermophoresis (MST) Binding Measurements

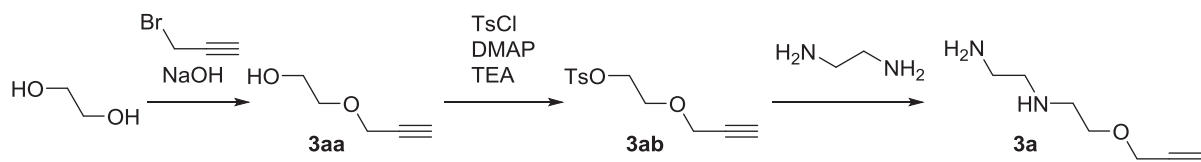
MST measurements were performed on a Monolith NT.115 system (NanoTemper Technologies) using the intrinsic fluorescent signal from compound **3**. The samples were prepared in MST buffer containing 50 mM Tris-HCl, pH 7.4, 150 mM NaCl, 5 mM MgCl₂ and 0.05 (v/v) % Tween-20. The concentration of compound was kept constant at 150 nM. The following RNA constructs were ordered from GE Healthcare Dharmacon for use in MST studies: miR-21 hairpin (A+U Bulge): GUUGACUGUUGAAUCUCAUGGCAAC; miR-21 A bulge: GUUGACUGUUGAAUCUCAUGGCAAC; miR-21 Base Paired Control: GUUGACUGUUGAAUCUCAUGGCAAC. RNA was titrated in 1:1 dilutions beginning at 20 μM and then samples were filled into in premium-coated capillaries. The measurement was performed at 40% LED and 20 to 80% MST power, with a Laser-On time of 30 s and Laser-Off time of 5 s, detecting fluorescence at Ex: 605–645 nm, Em: 680–685 nm. The data were analyzed by thermophoresis analysis, and fitted by the quadratic binding equation in MST analysis software (NanoTemper Technologies). The dissociation constant was then determined using a single-site model to fit the curve.

Chemical Synthesis

Abbreviations

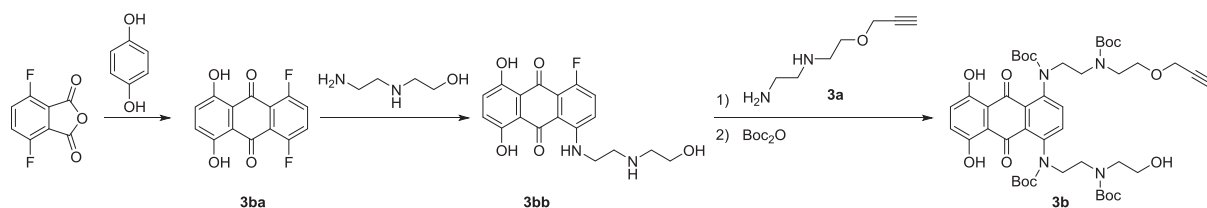
Boc, tert-butyloxycarbonyl; oxyma, Ethyl (hydroxyimino)cynoacetate; DCM, dichloromethane; DMAP, 4-Dimethylaminopyridine; DMF, *N,N*-dimethylformamide; DIC, *N,N'*-Diisopropylcarbodiimide; DIEA, *N,N*-Diisopropylethylamine; MS(ESI), mass spectrometry (electrospray ionization); HATU, 1-[Bis(dimethylamino)methylene]-1H-1,2,3-triazolo[4,5-b]pyridinium 3-oxide hexafluorophosphate; HOAt, 1-hydroxy-7-azabenzotriazole; HPLC, high performance liquid chromatography; MeOH, methanol; NMR, nuclear magnetic resonance; TEA, Triethylamine; TFA, trifluoroacetic acid; Ts, *p*-toluenesulfonyl.

Synthesis of *N'*-(2-(prop-2-yn-1-yloxy)ethyl)ethane-1,2-diamine (**3a**)



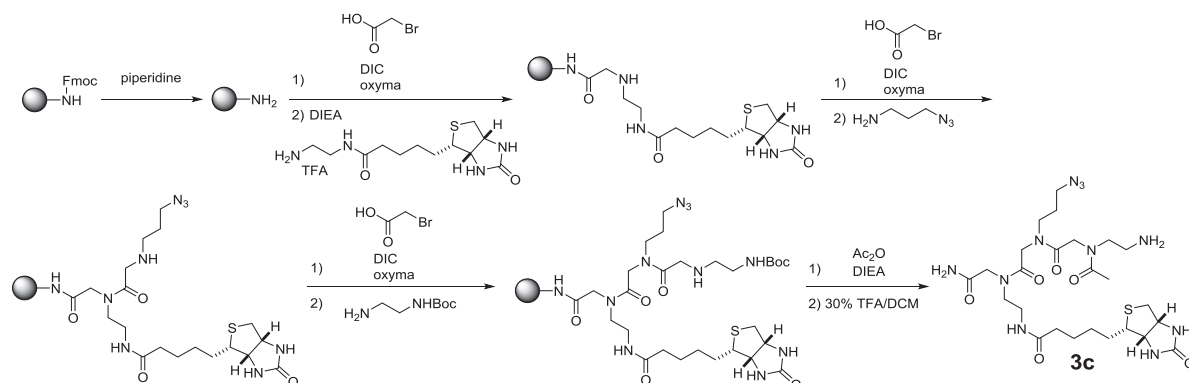
Both 2-(prop-2-yn-1-yloxy)ethan-1-ol (**3aa**) and 2-(prop-2-yn-1-yloxy)ethyl 4-methylbenzenesulfonate (**3ab**) were prepared according to Cserép et al. and McConnell et al. (Cserép et al., 2014; McConnell et al., 2010). To a solution of 2-(prop-2-yn-1-yloxy)ethyl 4-methylbenzenesulfonate (**3ab**) (5400 mg, 21 mmol) in MeOH (30 mL) was added dropwise ethylenediamine (20 mL, 300 mmol) at 0°C. After the addition of ethylenediamine, the reaction mixture was stirred overnight. Then, 10% K₂CO₃ was added to the reaction mixture, which was extracted with DCM. The combined organic layers were dried over Na₂SO₄ and concentrated *in vacuo*. The residue was purified by distillation (85°C / < 1 mmHg) to afford 1.6 g of **3a** (53% yield), a colorless oil. ¹H NMR(400 MHz, CDCl₃) δ 4.17–4.16 (m, 2H), 3.65 (t, *J* = 5.1 Hz, 2H), 2.85–2.80 (m, 4H), 2.69 (t, *J* = 7.8, 2H), 2.44–2.43 (m, 1H) 1.34 (br s, 3H). ¹³C NMR(100 MHz, CDCl₃) δ 41.8, 49.1, 52.5, 58.4, 69.5, 74.4, 79.7. MS *m/z* (ESI); calculated for C₇H₁₅N₂O (M + H)⁺ 143.1; found 143.3

Synthesis of Mitoxantrone Derivative **3b**



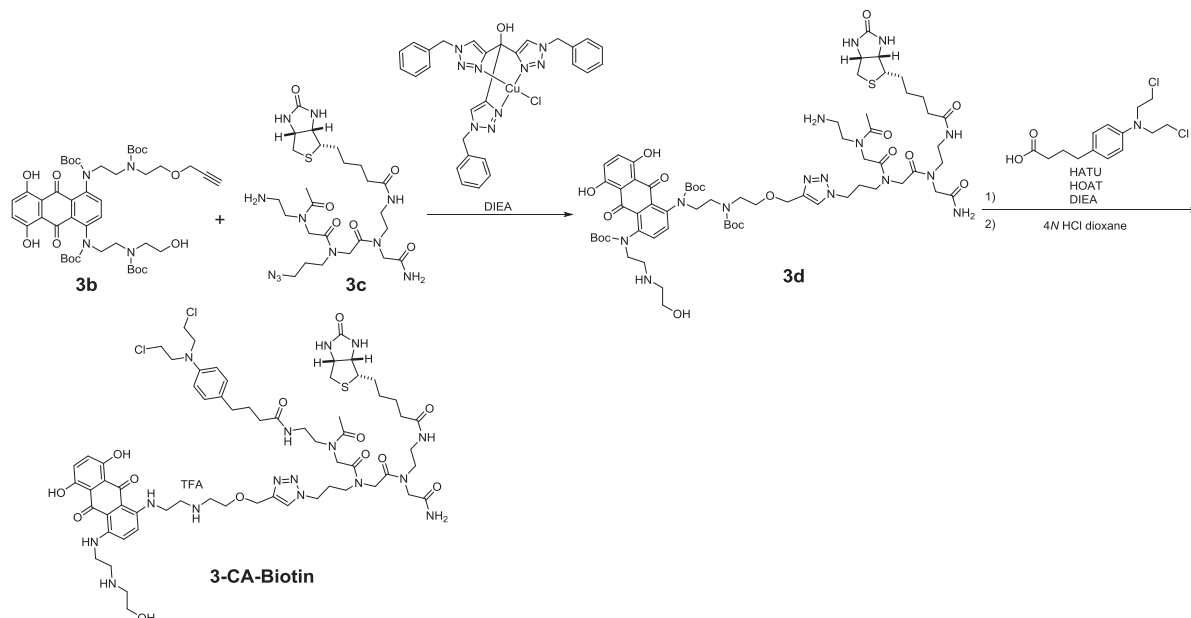
The compounds 1,4-difluoro-5,8-dihydroxyanthracene-9,10-dione (**3ba**) and 1-fluoro-5,8-dihydroxyanthracene-9,10-dione (**3bb**) were prepared according to Liu et al. and Mansour et al. (Liu et al., 2009; Mansour et al., 2010). To a solution of **3bb** (50 mg, 0.14 mmol) in pyridine (4 mL) was added **3a** (36 mg, 0.25 mmol). Then the mixture was stirred at 100°C under argon for 2 h. The reaction mixture was cooled to room temperature. Boc₂O (283 mg, 1.3 mmol) was added, and the reaction mixture was stirred overnight. The reaction mixture was evaporated and the residue was purified by silica gel column chromatography (15–60% ethyl acetate in hexane) to afford 50 mg of **3b** (43% yield) as a dark blue powder. ¹H NMR(CD₃OD, 700 MHz) δ 7.51–7.49 (m, 1H), 7.46–7.40 (m, 2H), 7.38–7.27 (m, 1H), 4.21–4.19 (m, 2H), 3.68–3.62 (m, 8H), 3.50–3.47 (m, 6H), 3.38–3.36 (m, 2H), 2.88 (s, 1H), 1.58 (s, 18H), 1.48 (s, 9H), 1.40–1.39 (m, 9H). ¹³C NMR(175 MHz, CD₃OD) δ 181.9, 157.3, 157.2, 157.1, 152.8, 149.3, 147.3, 147.2, 147.1, 129.2, 128.7, 125.2, 125.0, 124.9, 124.8, 111.1, 111.0, 84.6, 81.6, 81.5, 81.4, 81.3, 80.7, 76.2, 69.8, 69.6, 61.5, 61.3, 59.2, 52.1, 51.3, 41.8, 41.3, 28.8, 28.7, 28.2. HRMS *m/z* (ESI): calculated for C₄₅H₆₃N₄O₁₄ (M + H)⁺ 883.4341, found 883.4375.

Synthesis of the Peptoid Backbone (3c)



Rink amide resin (400 mg, 0.23 mmol) was swollen in DMF at room temperature for 10 min and then deprotected with a solution of 20% piperidine in DMF (5 mL, 2 x 20 min). The resin was washed with DMF (3 x 5 mL). To the resin were added 1.1 mL of 1.0 M bromoacetic acid in DMF, DIC (0.3 mL, 1.2 mmol) and oxyma (163 mg, 1.1 mmol), and the mixture was shaken at room temperature for 2 h. The resin was washed with DCM (5 x 6 mL) and DMF (5 x 6 mL). Then to the resin was added a solution of N-(2-aminoethyl) biotinamide (384 mg, 1.0 mmol) in DMF (2 mL) and DIEA (0.2 mL, 1.2 mmol), and the mixture was shaken at room temperature for 1.5 h. The resin was washed with DCM (5 x 6 mL) and DMF (5 x 6 mL). Then to the resin were added 1.1 mL of 1.0 M bromoacetic acid in DMF, DIC (0.3 mL, 1.2 mmol) and oxyma (163 mg, 1.1 mmol) and the mixture was shaken at room temperature for 2 h. The resin was washed with DCM (5 x 6 mL) and DMF (5 x 6 mL). Then to the resin were added DMF (2 mL), 3-azidopropan-1-amine (230 mg, 2.3 mmol). The mixture was shaken at room temperature overnight. The mixture was washed with DCM (5 x 6 mL) and DMF (5 x 6 mL). Then to the resin were added 1.1 mL of 1.0 M bromoacetic acid in DMF, DIC (0.3 mL, 1.2 mmol) and oxyma (163 mg, 1.1 mmol), and the mixture was shaken at room temperature for 2 h. The resin was washed with DCM (5 x 6 mL) and DMF (5 x 6 mL). Then to the resin were added DMF (2 mL), *N*-Boc-ethylenediamine (184 mg, 1.2 mmol) and DIEA (0.2 mL, 1.2 mmol), and the mixture was shaken at room temperature for 1 h. The beads were washed with DCM (5 x 6 mL) and DMF (5 x 6 mL) followed by addition of DMF (4 mL), acetic anhydride (0.12 mL 1.3 mmol) and DIEA (0.4 mL, 2.3 mmol). The mixture was shaken at room temperature for 1 h followed by washing the resin with DCM (5 x 6 mL) and DMF (5 x 6 mL). Then to the resin was added 30% TFA in DCM (2 mL), and the mixture was shaken at room temperature for 30 min. The mixture was filtered, and the filtrate was evaporated. The crude product was purified by preparative HPLC (linear gradient of 0% to 100% CH₃OH in H₂O with 0.1% (v/v) TFA over 60 min) to afford compound **3c** as a colorless oil (8 mg, 4.8% yield). HRMS *m/z* (ESI): calculated for C₂₅H₄₄N₁₁O₆S (M + H)⁺ 626.3197, found 626.3216.

Synthesis of 3-CA-Biotin (10)



To a solution of **3b** (57 mg, 0.065 mmol) and **3c** (51 mg, 0.082 mmol) in DMSO (0.6 mL) were added Cu(I)-catalyst (7.5 mg, 0.0048 mmol) and DIEA (0.5 mL, 2.9 mmol). The reaction mixture was stirred at 60°C overnight. Then saturated NaHCO₃ was added, the aqueous layer was extracted with DCM, and the organic layer was evaporated. The residue was purified by silica gel column chromatography (0–5% MeOH with 1% NH₃ aq in DCM) to afford 70 mg of **3d** (partially purified).

To a solution of **3d** (24 mg, 0.016 mmol) in DCM were added chlorambucil (42 mg, 0.14 mmol), HOAt (19 mg, 0.14 mmol), HATU (53 mg, 0.14 mmol) and DIEA (40 μL, 0.23 mmol). The reaction mixture was stirred at room temperature overnight and then evaporated. To the residue was added 4N HCl dioxane (3 mL) and the mixture was stirred at room temperature for 2 h followed by evaporation of the suspension. The residue was diluted with water (3 mL) and the aqueous layer was washed with DCM and ethyl acetate. The aqueous layer was directly purified by preparative HPLC with a linear gradient of 0–100% acetonitrile in H₂O with 0.1% TFA over 60 min. Fractions containing the compound were concentrated *in vacuo* and the residue was dissolved in 200 μL of DMSO. The concentration of the DMSO stock solution (1.69 mM, 200 μL, 2.1% yield) was determined with 10 mM Tris-HCl, pH 7.4 and molecular extinction coefficient of mitoxantrone hydrochloride (19200 M⁻¹ cm⁻¹ at 608 nm) (Hajihassan and Rabbani-Chadegani, 2011). Purity was analyzed on an analytical HPLC with a linear gradient of 0–100% acetonitrile in water with 0.1% TFA (see Figure S6). HRMS m/z (ESI): calculated for C₆₄H₉₁Cl₂N₁₆O₁₃S (M + H)⁺ 1393.6049, found 1393.6036.

QUANTIFICATION AND STATISTICAL ANALYSIS

All plots show means with error bars representing S.E.M., unless dictated otherwise. Experiments were completed at least in triplicate. Data were plotted using Graphpad's Prism 7.

DATA AND SOFTWARE AVAILABILITY

The Informa software is free for academic use with a software license agreement. Please see: <https://disney.florida.scripps.edu/software/>.